

DEEP INELASTIC MUON SCATTERING ON CARBON AT LARGE Q^2

D. Bollini, P.L. Frabetti, G. Heiman, L. Monari, F.L. Navarria
Istituto di Fisica dell'Università-Bologna, Italy
INFN -- Sezione di Bologna, Italy

A.C. Benvenuti, M. Bozzo, R. Brun, H. Gennow, M. Goossens,
D. Reeder, C. Rubbia, D. Schinzel
CERN -- Geneva, Switzerland

D. Barden, J. Cvach, N. Fadeev, I. Golutvin, I. Ivanchenko
Y. Kiryushin, M. Klein, V. Krivokhizhin, V. Kukhtin,
V. Kisselev, W. Nowak, I. Savin, D. Smolin, G. Vesztergombi
A. Volodko, A. Zarubin, V. Grushin, A. Shikanyan
Joint Institute for Nuclear Research, Dubna, USSR

D. Jamnik, U. Meyer-Berkhout, F. Navach, A. Staude
K.M. Teichert, R. Tirlir, R. Voss, C. Zupancic
Sektion Physik der Universität-München, Federal Republic of Germany

J. Feltesse, J. Maillard, J.M. Malasoma, A. Milsztajn,
J.F. Renardy, Y. Sacquin, G. Smadja,
M. Virchaux, P. Verrecchia
D. Ph. PE, CEN -- Saclay, France

Presented by A.C. Benvenuti

Summary

Preliminary results are presented on the deep inelastic scattering of μ^+ on carbon at 120 and 280 GeV incoming energies. The Q^2 range covered is from 30 to 200 (GeV/c)². The structure function F has been calculated using a sample of 29000 μ^+ at 120 GeV and 10,000 μ^+ at 280 GeV.

The results are in agreement with the measurements performed with neutrino beams. An upper limit for the production of the T by high energy muons is also given.

Introduction

The CERN SPS NA4 experiment¹ was designed to extend the systematic study of deep inelastic muon scattering to the highest Q^2 made available by the high intensity muon beam at the SPS.

In order to overcome the drastic loss of the event rate due to the photon propagator, the experiment must have a very large luminosity. This was obtained in the present experiment by surrounding the target with a focusing toroid. The properties of this system (Fig. 1) are:

a) Scaling Invariance

The sagitta Δ of the muon in the toroid is approximately given by

$$\Delta = \frac{M_p}{0.3B} \frac{Q^2}{Q_{\max}^2} \quad \text{The units are: GeV, tesla, meters}$$

hence for a given toroid radius the spectrometer will always confine a fixed percentage of the maximum Q^2 available, independently of the beam energy.

b) Q^2 Selectivity

The Q^2 range of the trigger is determined simply by requiring that the μ had an excursion greater than Δ_{\min} in the toroid. This is of great importance in order to obtain high statistics at high Q^2 due to the $1/Q^4$ fall off of the cross section.

1. The Muon Beam

The muon beam is schematically illustrated in Fig. 2. Briefly the hadrons produced at zero degree angle are collected, momentum selected and then injected into a decay channel 600 meters long. A Beryllium absorber located at the end of the decay region provides a rejection factor of 10^8 against hadrons. The muons are then momentum analyzed and transported to the experimental hall. A set of magnets in front of the NA 4 spectrometer provides the necessary bending power to restore the beam on-axis with the 50 meter long spectrometer after the bending introduced by the European Muon Collaboration (EMC) spectrometer (Fig. 3).

The salient parameters of the CERN SPS muon beam are:

- The very high flux which is due to the long decay channel and to the presence of lenses within the channel that insure the capture of the decay muons. Typically the muon yield is $1.8 \times 10^{-6} \mu^+/p$ at 280 GeV muon energy, with 400 GeV protons.
- The low intensity halo which is of the order of 10% of the primary beam at 280 GeV.
- The excellent muon momentum definition $\Delta p/p \sim .5\%$ which is provided by a set of hodoscopes in front and behind the last bending magnet.

2. The Experimental Apparatus

The experimental apparatus, shown in Fig. 4, consists of a beam defining hodoscope, a veto wall which eliminates the halo muons, the target spectrometer and the forward detector.

The spectrometer is made of ten identical iron toroids (supermodules) with interspersed liquid scintillator counters and multiwire proportional chambers to detect and track the scattered muon.

The toroids provide a field which varies from 2.1 T at the center to 1.7 T at the outer edge. A five meter long target is housed in the central hole of each toroid. Three target types are available: hydrogen, deuterium and carbon.

Each supermodule, see Fig. 5a, is composed of eight modules each comprising four iron discs 110 mm thick with outer diameter of 275 cm and inner diameter of 50 cm.

With these dimensions and taking into account the dilution in bending power introduced by the air gaps, the spectrometer can contain 50% of the maximum Q^2 attainable at any given beam energy. Higher Q^2 can still be measured albeit with poorer resolution.

MWPC planes (two chambers/plane) each measuring one spatial coordinate with ± 2 mm accuracy are inserted after each module while the trigger counters are located every four modules.

The chambers are rectangular in shape with dimensions 1.5 m x 3 m and a central hole to allow for the passage of the beam (Fig. 5b).

The trigger counters are semi-circular in shape and are subdivided into seven half-rings spanning uniformly from an inner diameter of 58 cm to an outer diameter of 270 cm (Fig. 5c). The light is collected at both ends of the half-rings and the PM pulses are sent after discrimination to mean-timers to minimize the time variation due to the different impact points of the muon in the counter.

A set of five beam defining hodoscopes with a mosaic structure (Fig. 6), designed to withstand fluxes of up to 10^9 muons/burst are installed in the spectrometer. They are used to correlate the beam muon which initiated the trigger with the momentum defining hodoscopes installed in the beam line and to the target section where the interaction occurred. The time of flight of each element of the hodoscopes is measured with an accuracy of one-half nanosecond at the occurrence of each trigger. Furthermore, they are used to monitor the beam flux and the steering of the beam through the apparatus, which is very important given the length of the

spectrometer. The first of these hodoscopes is also used as "beam counter" in the trigger logic.

A bending magnet with bending power of 7 T-m is situated at the end of the spectrometer and is used to deflect the muons which have undergone a low Q^2 interaction ($Q^2 < 4(\text{GeV}/c)^2$) into a muon identifier 25 m downstream (Forward Detector). The Forward Detector accepts muons within 30 - 130 GeV/c, at 280 GeV incident beam energy.

3. The Distributed Trigger

The trigger configuration is shown in Fig. 7. Briefly the output of each half-ring in a trigger plane is combined by a remotely controlled OR unit to give a "plane signal". This information is then transmitted through a fast rigid copper conductor called a high-way ($\beta = 0.99$) to the neighbouring supermodules. The trigger is then configured independently at each supermodule by sampling the information from six consecutive counter planes which is available synchronously with the beam and halo information via the fast high-way. Upon occurrence of a trigger, a strobe signal is generated and distributed to the chambers of each supermodule via the high-way.

For the data which will be presented here, the trigger was defined as the coincidence of four consecutive planes with a beam particle not accompanied by a halo particle. The Q^2 selectivity is obtained by changing the ring configuration in the trigger counters.

The acceptance of this trigger for two modes of running, full-plane (rings 1-7), and plane without the innermost ring (rings 2-7) is given in Fig. 8(a,b) respectively for a 120 GeV/c muon beam. In either case the acceptance is seen to be rather uniform in the Q^2 region covered by the trigger. The full-plane trigger has a Q^2 cut off of 10 $(\text{GeV}/c)^2$ due to the geometry of the apparatus which is raised to 20 $(\text{GeV}/c)^2$ by removing ring one from the trigger.

Typical trigger rates per muon unaccompanied by halo particles are 10^{-4} and 10^{-5} respectively for the two trigger conditions and eight carbon targets which yield a luminosity of $5 \cdot 10^{27} \text{ cm}^{-2} \times \text{nucleon per incoming muon}$.

The fraction of deep inelastic events is typically 15%, the bulk of the triggering rate being given by events without a visible muon which are produced by hadronic and/or electromagnetic shower penetration in the trigger counters.

4. Spectrometer Resolution

The momentum resolution has been measured to be 8% rms from the energy spread

of a 100 GeV muon beam displaced into the spectrometer. The resolution is independent of the muon momentum above ~ 20 GeV/c.

The estimated Q^2 resolution (Fig. 9) varies from 10% at 20 (GeV/c) to $\sim 6\%$ at 200 (GeV/c)² for focused tracks and is somewhat worse for the defocused ones.

5. Production of Heavy Vector States

The muon beam is used as an intense source of virtual photons which produce vector states of the J/ψ or T type. These events will then be detected as multimMuon events through their decays to $\mu^+\mu^-$.

The acceptance of the spectrometer is of the order of 1% at the J/ψ and of 48% in the T region. The mass resolution is 10% at the T mass and does not depend appreciably on the dimuon mass.

In a data set taken with 280 and 250 GeV/c incoming μ^+ a total of 971 events were observed for $1.50 \cdot 10^{11}$ gated muons. An analysis of a part of this sample has been presented elsewhere.²⁾ After cuts on the vertex reconstruction and on the track quality 761 events were left, of these 11% had a third μ^+ in the forward detector. The total number of trimuon events is much larger but the leading muon escapes detection due to the small acceptance of the forward detector. A typical trimuon event is shown in Fig. 10.

In addition there were 18 $\mu^-\mu^-$ and 39 $\mu^+\mu^+$ events. The contribution of π/K decays to the $\mu^+\mu^-$ sample can be estimated from the observed number of $\mu^-\mu^-$. If these events are all ascribed to this process we expect 10% contamination in the $\mu^+\mu^-$ sample. No conclusion can be drawn from the $\mu^+\mu^+$ sample which is heavily contaminated by halo muons. The $\mu^+\mu^-$ mass spectrum is shown in Fig. 11. The most important contributions to the mass spectrum are the leptonic decay of vector states and the electromagnetic trident (EMT) production by the Bethe-Heitler and Compton processes (Fig. 12). The total cross-section for EMT has been calculated to be $7 \cdot 10^{-33}$ cm² on proton and $1.5 \cdot 10^{-32}$ cm²/nucleon on carbon targets. EMT on carbon are produced via three processes: coherent scattering on the whole nucleus, quasi-elastic scattering on individual nucleons and inelastic scattering. The contribution of each mechanism to the total cross-section is of comparable importance in our experiment. In each case the Bethe-Heitler process is about one order of magnitude more important than the Compton process and their interference. The EMT cross-section as a function of the dimuon mass varies from $\sim 10^{-34}$ cm²/GeV at 2.5 GeV to 10^{-40} cm²/GeV at 16 GeV. Fig. 11 shows the EMT cross-section calculated taking into account the apparatus acceptance and luminosity.

The dimuon spectrum measured in this experiment is compatible with the EMT production for masses greater than 5 GeV. In this mass range we observe 161 events as contrasted to 150 predicted by the EMT processes. In the restricted mass region 8-12 GeV around the T mass the number of events observed and number calculated assuming EMT production is 24 and 30 respectively. From this we can calculate an upper limit for the T production cross-section:

$$\sigma_T \times \text{BR}(T \rightarrow \mu^+\mu^-) \leq 0.6 \cdot 10^{-38} \text{ cm}^2/\text{nucleon}$$

at the 90% confidence level.

The overall systematic error on this value is about 50%. This result is compatible with the estimate which is obtained from the branching ratio³⁾ of 2% for $T \rightarrow \mu\mu$ and the theoretical prediction⁴⁾ of 10^{-34} cm² for the T photoproduction cross-section which gives for $\sigma_T \sim 0.5 \cdot 10^{-36}$ cm² in μ production.

The contribution of the J/ψ to the $\mu^+\mu^-$ mass spectrum has been calculated to be 400 ± 150 events in our apparatus using the cross-section for $\mu \text{Fe} \rightarrow J/\psi + X$ which has been recently measured (5) to be 0.76 ± 0.22 nanobarns/nucleon and the known branching ratio of 7% to $\mu^+\mu^-$. This is in good agreement with the observed value of 442 events in the mass region 2-4 GeV/c².

In conclusion the observed $\mu^+\mu^-$ mass spectrum can be interpreted as being produced by the J/ψ decays and the standard EM tridents.

6. Deep Inelastic Scattering

The results presented here are based on two data samples taken with 280 and 120 GeV μ^+ . The 280 GeV sample ($\sim 15\%$ of the total) contains $\sim 10,000$ μ^+ scattered with $Q^2 > 50$ (GeV/c)² for $1.3 \cdot 10^{10}$ incoming μ^+ and was taken during the initial phase of the experiment. The 120 GeV sample ($\sim 10\%$ of the total) contains 29,000 μ^+ scattered with $Q^2 > 25$ (GeV/c) for $1.7 \cdot 10^{10}$ incoming μ^+ and has been taken during June 1979. For this sample only the data taken with a high Q^2/Q_{MAX}^2 trigger has been included in the present analysis.

We have studied the possible contamination by background events in the data. The main sources of this background in the deep inelastic events are decay muons from the hadrons produced in the interaction and unrecognized halo muons. The first background can be estimated from the events with one μ^- in the final state and no visible μ^+ . These events are observed to populate the region in the Q^2, ν plot (Fig. 13a) at low Q^2 and at high values of the hadronic energy (ν).

The corresponding background μ^+ in the deep inelastic sample have the same

characteristics as the single μ^- events and therefore are mostly concentrated in a kinematical region which is not being studied at present. For comparison the Q^2, ν plot of the 120 GeV sample is shown in Fig. 13b).

By applying a cut off in the minimum momentum of the scattered μ^+ at 15 and 20 GeV/c respectively for the 120 and 280 GeV sample the contribution of this background is reduced to the level of $\sim 1\%$. The background due to halo muons accidentally included in this sample as good events has been estimated by scanning a fraction of the data to be less than 1%. The presence of halo events in the sample can be easily detected by the shape of the azimuthal distribution which is strongly asymmetric for halo muons. There is no detectable asymmetry in the data sample considered here. A computer reconstruction of a typical event from the 120 GeV sample is shown in Fig. 14. The $d^2\sigma/dx dQ^2$ have been calculated for several (Q^2, x) bins with radiative corrections included. A value of 0.22 was used for the parameter $R = (\sigma_L/\sigma_T)$ in extracting the structure function. The $F_2(x, Q^2)$ per nucleon is given in Fig. 15 for the two data sets. The Q^2 range covered is between 30 to 200 $(\text{GeV}/c)^2$ and will be extended to lower and higher values of Q^2 when the analysis of the full sample is completed. The two data samples agree within an estimated overall normalization factor of 10%.

The comparison with F_2 as determined in neutrino-iron scattering⁶⁾ is shown in Fig. 15, after multiplying by 5/18 to take into account the difference between the weak and electromagnetic charges. The agreement between the two measurements is satisfactory. Our data give slightly higher values of F_2 at small x for the 120 GeV sample. This could be due to a residual overall normalization factor or to resolution effects which may not be fully corrected at this stage of the data analysis.

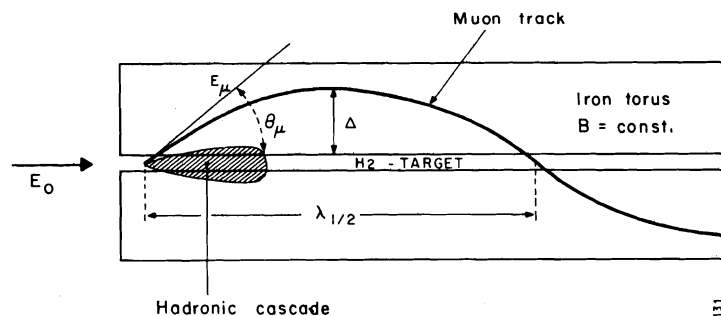
The kinematic region covered by the data presented allows a preliminary calculation of the moments $M(n, Q^2)$ of $F_2(x, Q^2)$ for $n = 4, 6$. In Fig. 16 Nachtmann moments are shown together with the results of Anderson et al.⁷⁾ which rely on a combination of SLAC and FNAL deuterium measurements. The given range of n and Q^2 arises from the requirement that more than 70% of the moment is covered by the data. The errors bars of $M(n, Q^2)$ include the statistical error to which 25% of the extrapolated contribution is added in quadrature.

The resulting moments appear to be a smooth continuation of the trend observed in deuterium scattering extending the Q^2 range up to about 120 $(\text{GeV}/c)^2$. This is also shown by the superimposed curve representing a QCD fit with second order corrections⁸⁾ to the deuterium data alone.

References

- 1) "NA4 Proposal", CERN/SPSC/74-79/P19, 1 August 1974, C. Rubbia et al.
- 2) J. Feltesse, High Energy Muon Interactions on Carbon, presented at the 14th Rencontre de Moriond, Les Arcs 1979; and, G. Smadja, Deep Inelastic Scattering of μ^+ at 280 GeV/c on Carbon, presented at the Specialized Seminars, Erice 1979.
- 3) PLUTO Collaboration, Ch. Berger et al., DESY report 79-19 (1979).
- 4) H. Fritzsche and K.H. Streng, Phys. Lett. 72B (1978) 385.
- 5) A.R. Clark et al., Phys. Rev. Lett. 43 (1979) 187.
- 6) J.G.H. de Groot et al., Zeit. Phys. C, Particle and Fields 1 (1979) 143.
- 7) H.L. Anderson et al., Fermilab Pub. 79/30-Exp.
- 8) D.A. Ross, N.B. Skachkov, Private Communication.

PRINCIPLE OF q^2 - FOCUSSED SPECTROMETER



$$\lambda_{1/2} = 6.66 p_1 / B$$

$$\Delta = \frac{M p}{0.3 B} \frac{q^2}{q_{\max}^2}$$

Fig. 1 - Distributed target concept.

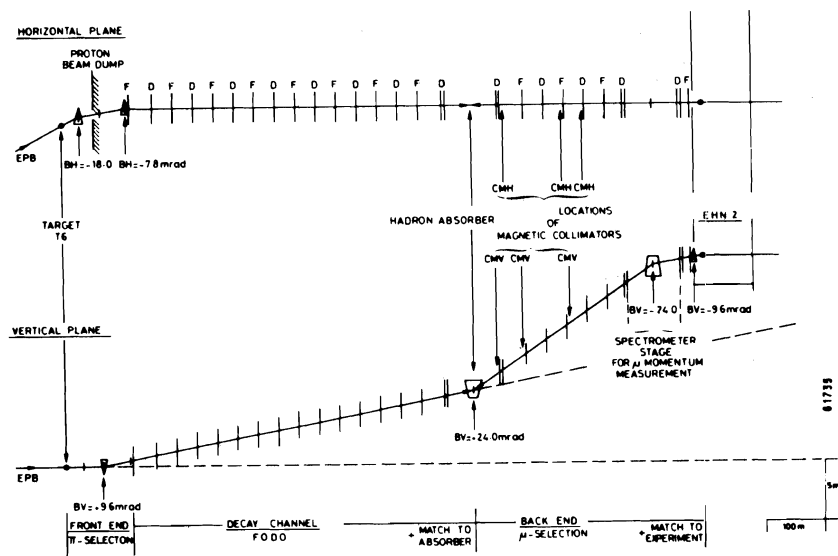


Fig. 2. SPS muon beam layout.

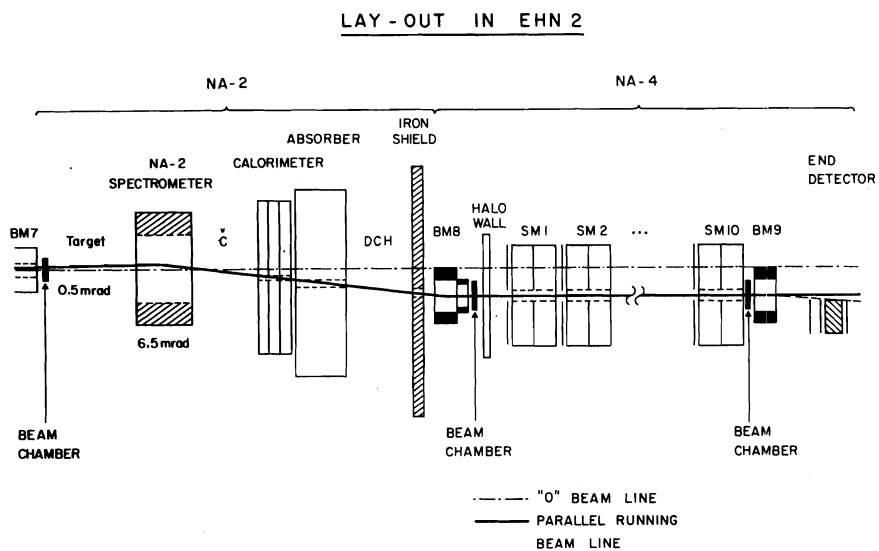


Fig. 3. Layout of the muon beam in the experimental hall.

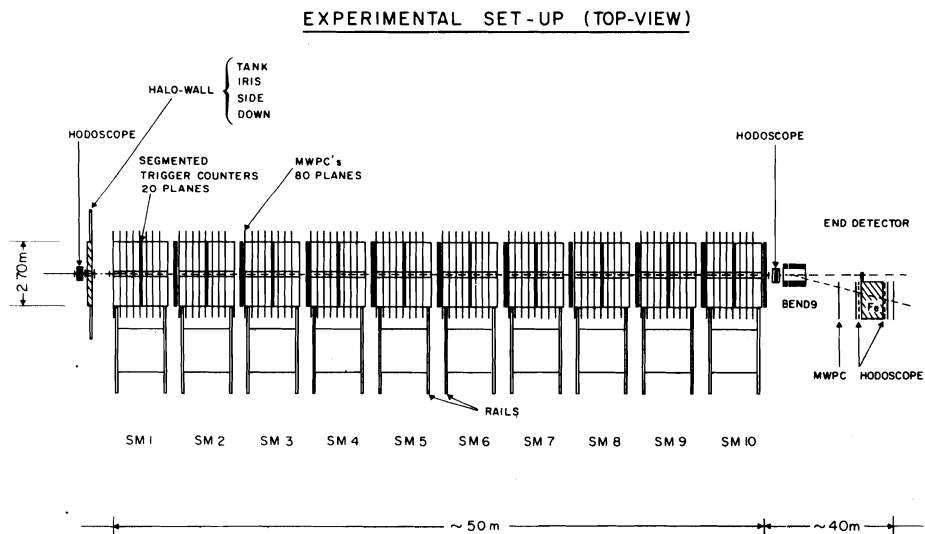


Fig. 4. The NA4 experimental apparatus.

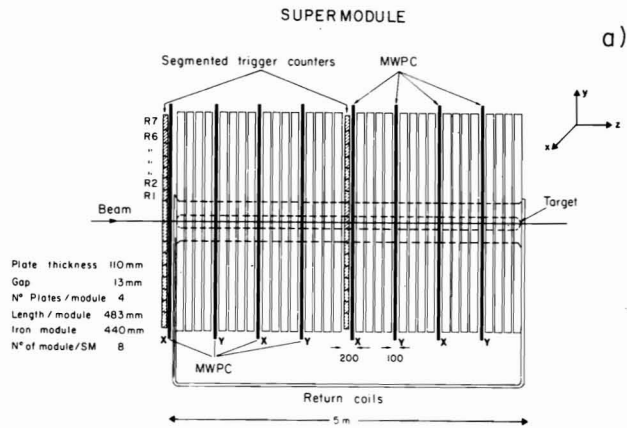


Fig. 5a. Detail of a Supermodule.

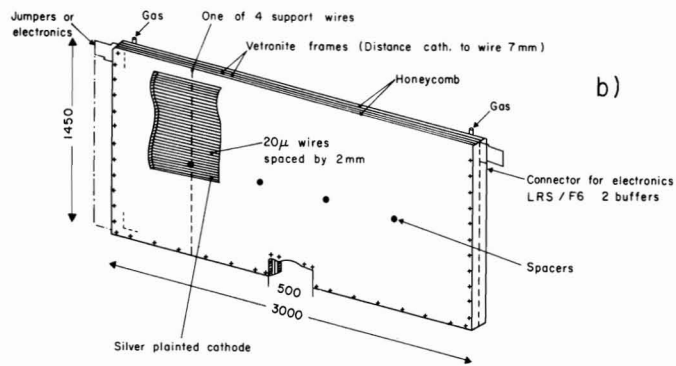


Fig. 5b. Detail of a MWPC.

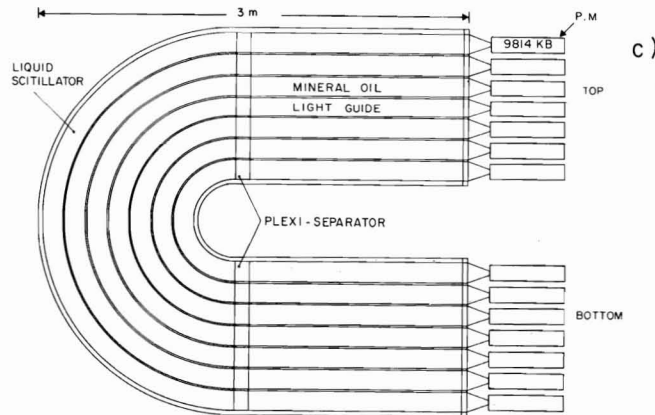


Fig. 5c. Detail of a trigger counter.

Plane 5

looking upstream

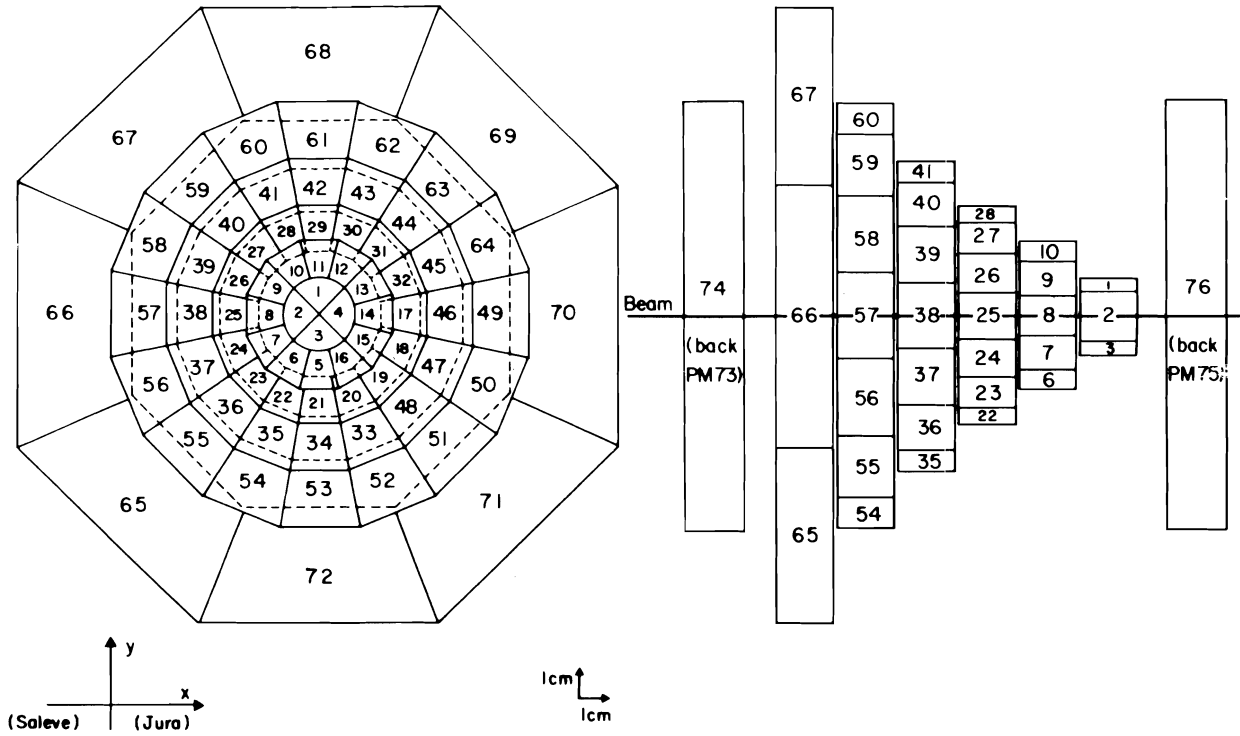


Fig. 6. High flux beam hodoscope.

Distributed Trigger

Halo wall

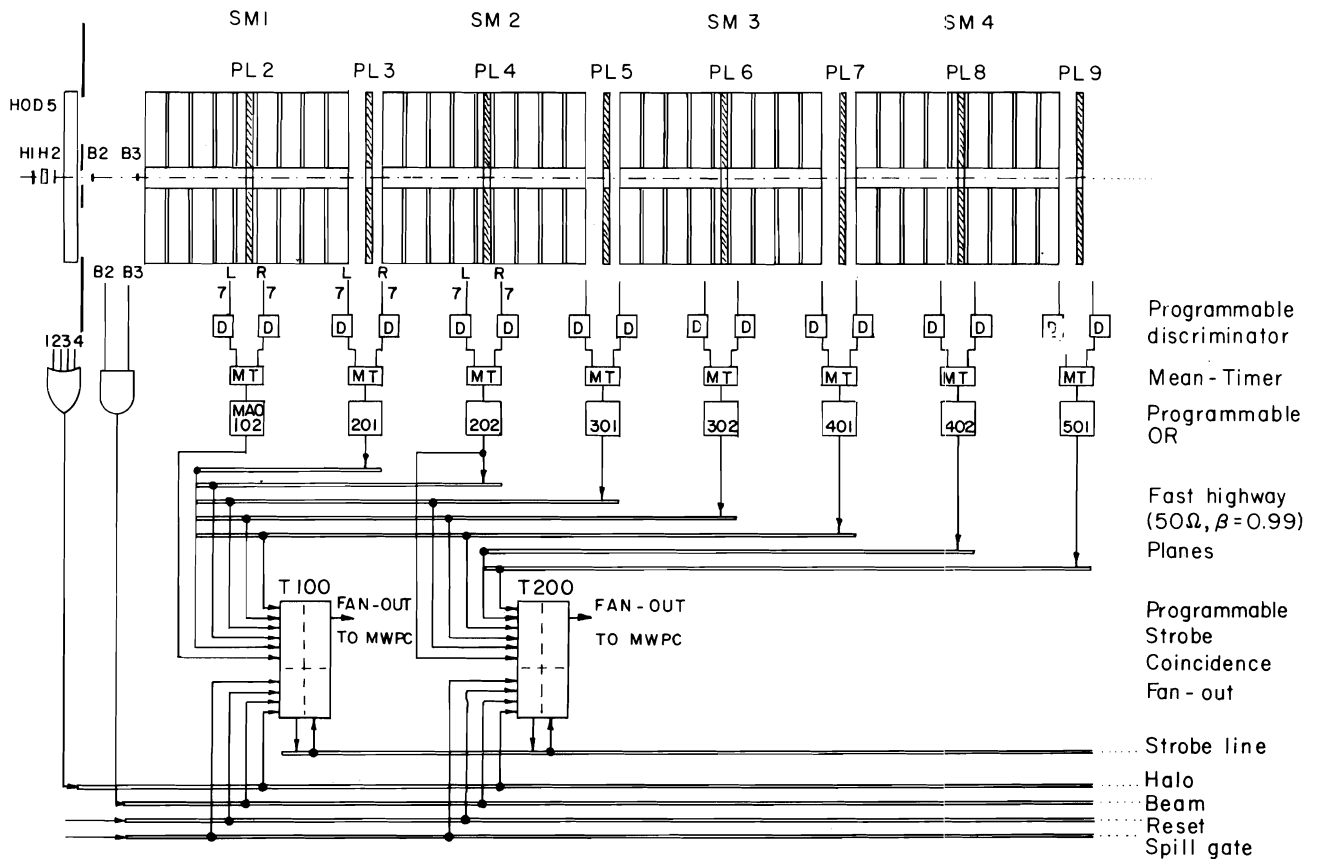


Fig. 7. The trigger configuration.

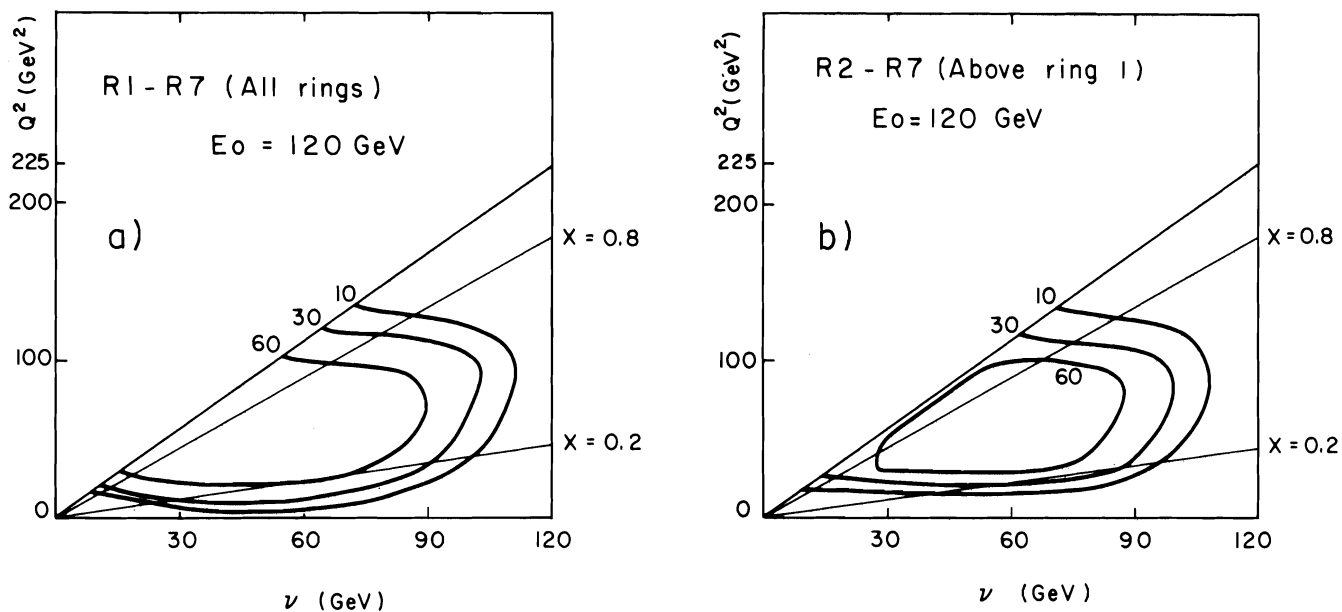


Fig. 8. Experimental acceptance with a 120 GeV beam: a) full plane trigger. b) rings 2 - 7 trigger

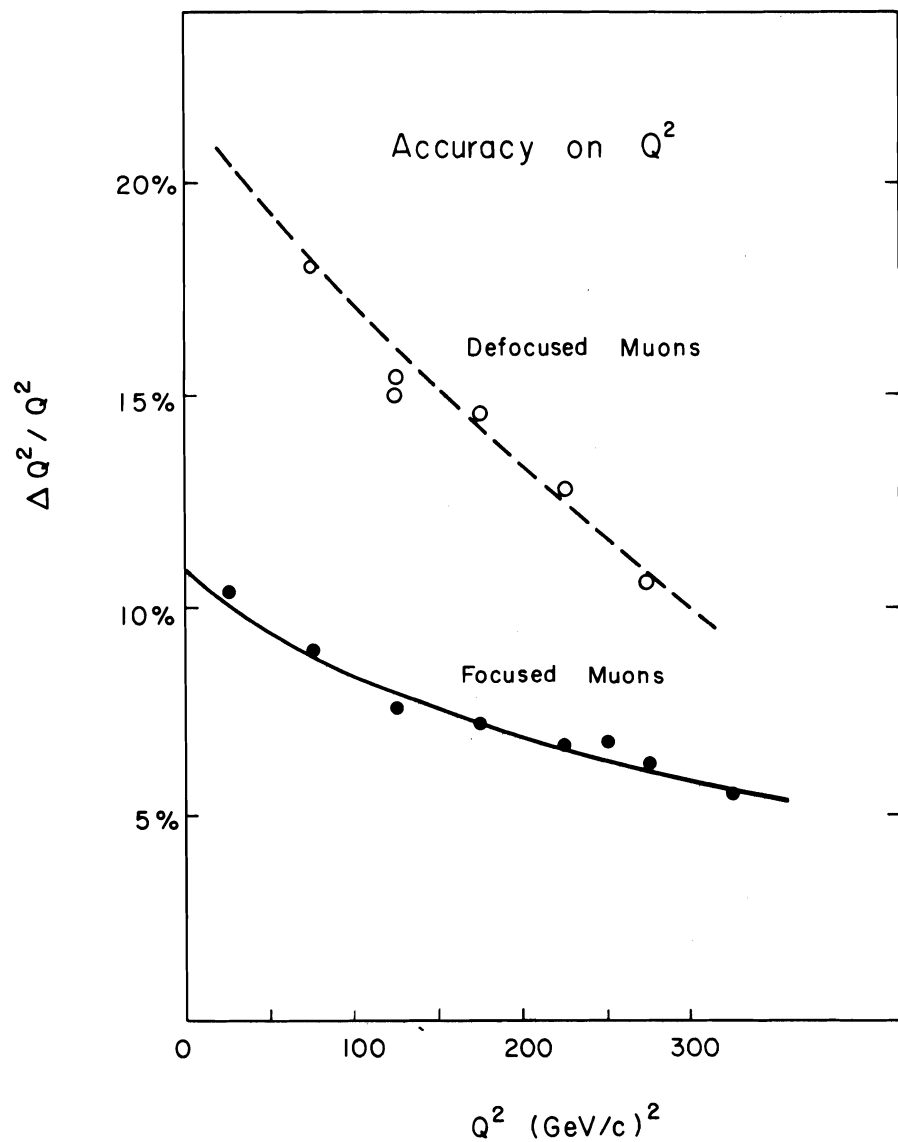


Fig. 9. Q^2 resolution for a beam energy of 280 GeV: a) for focused; b) for defocused.

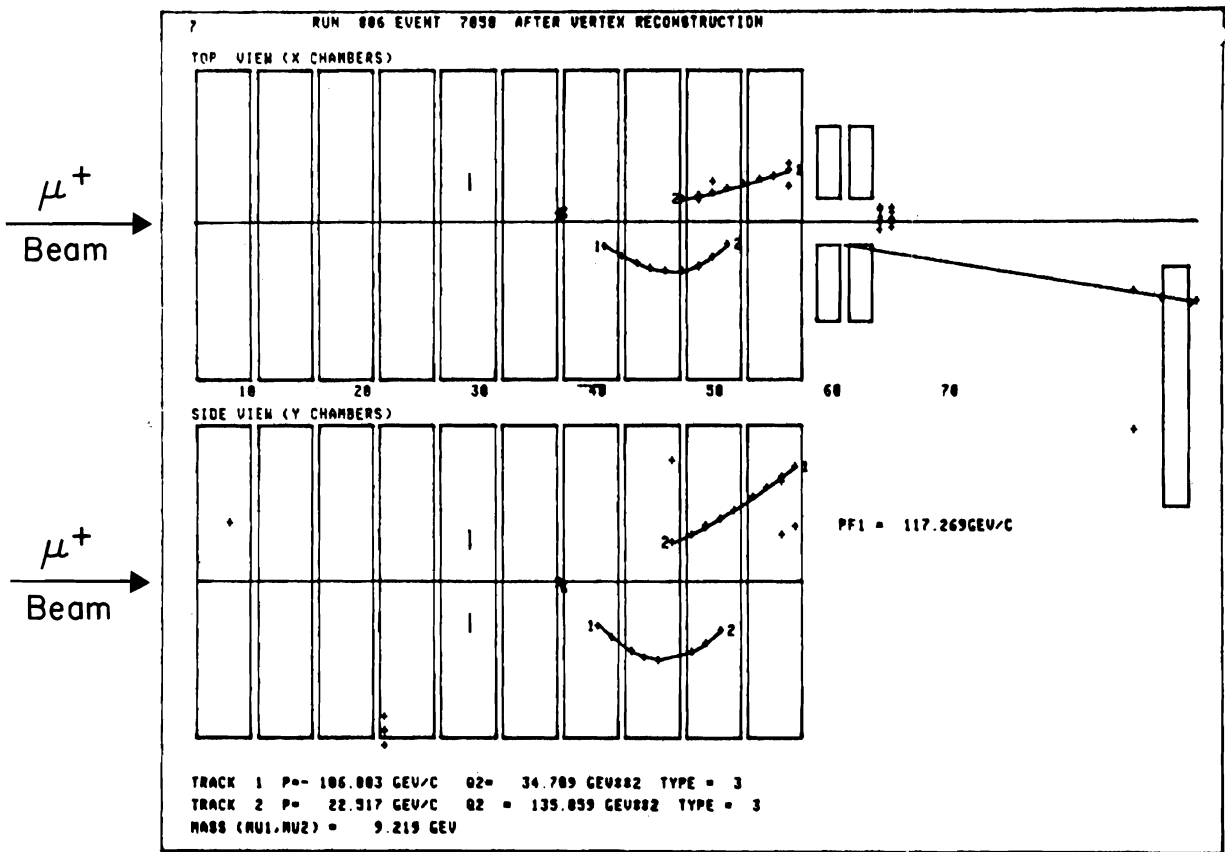


Fig. 10. Typical trimuon event.

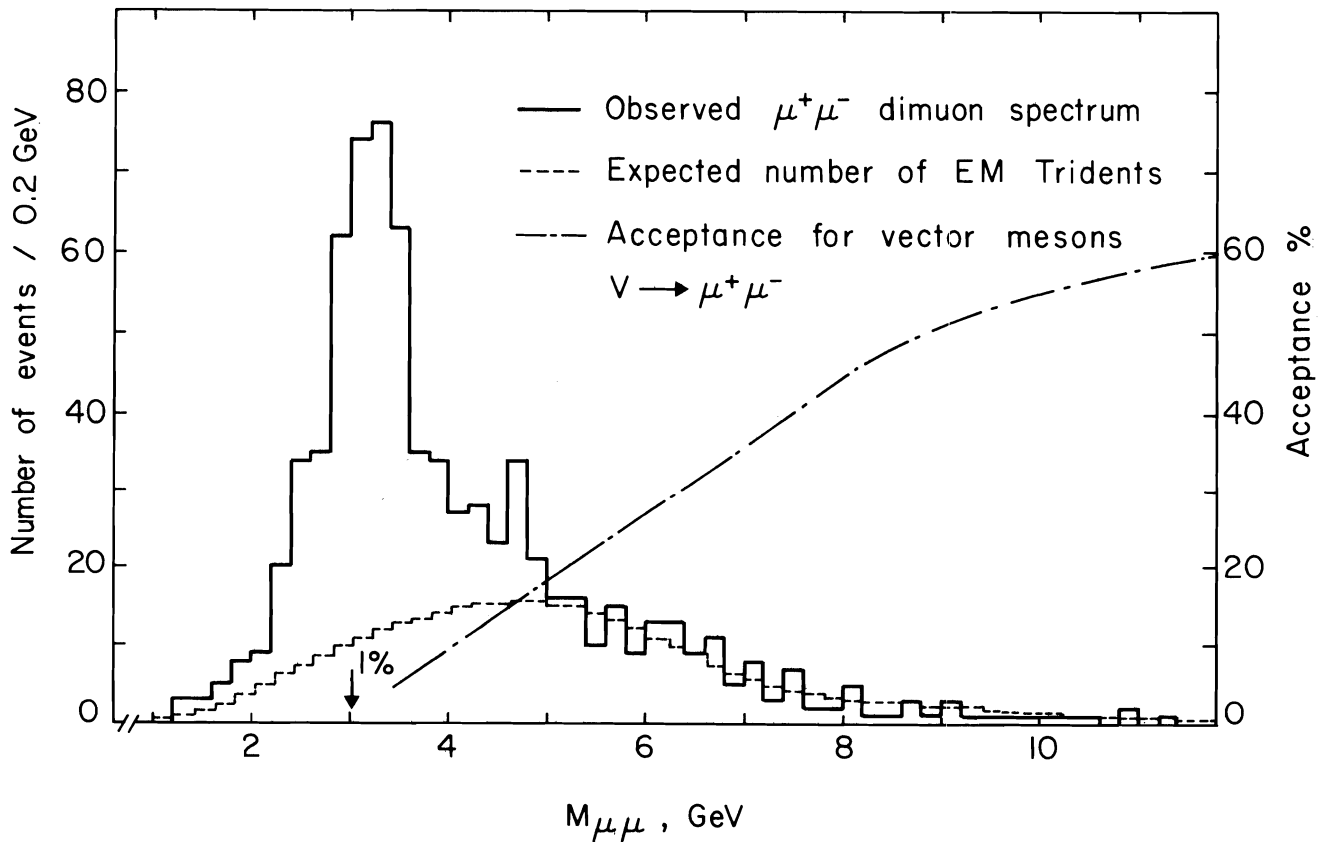


Fig. 11. $\mu^+\mu^-$ mass spectrum with superimposed the contribution from the EMT.

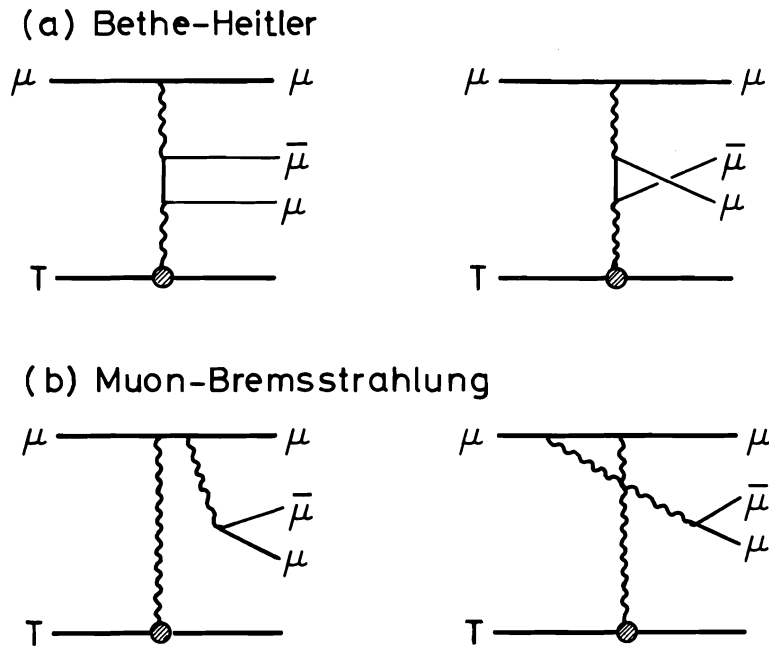


Fig. 12. Diagrams contributing to the EMT production.

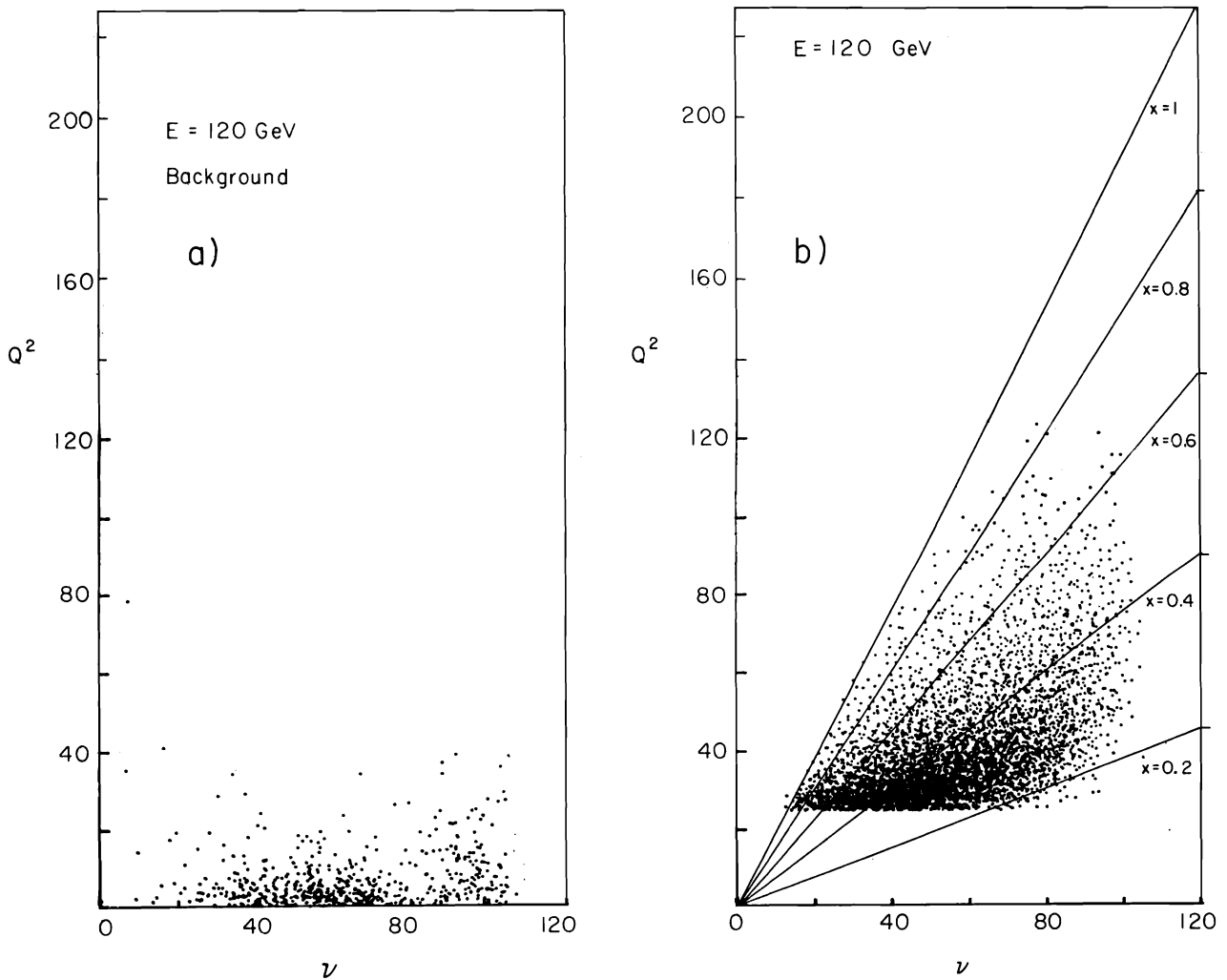


Fig. 13. Q^2 , ν plot for the 120 GeV sample: a) μ^- events. b) μ^+ events.

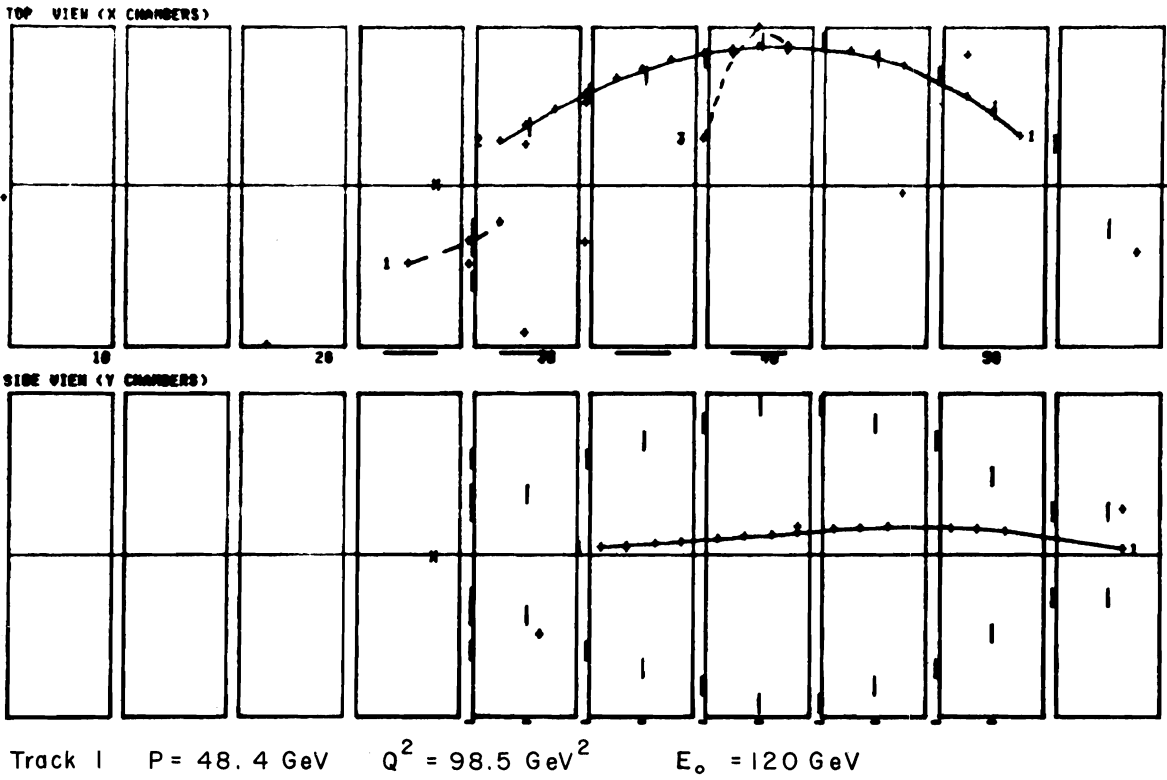


Fig. 14. Example of a deep inelastic muon scattering event at 120 GeV in the NA4 apparatus.

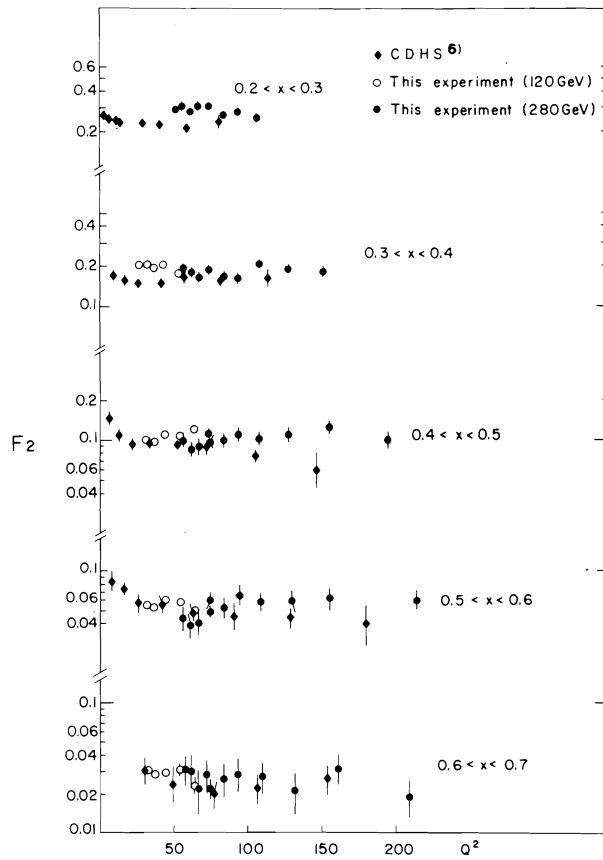


Fig. 15. Measurement of the structure function $F_2(Q^2, x)$.

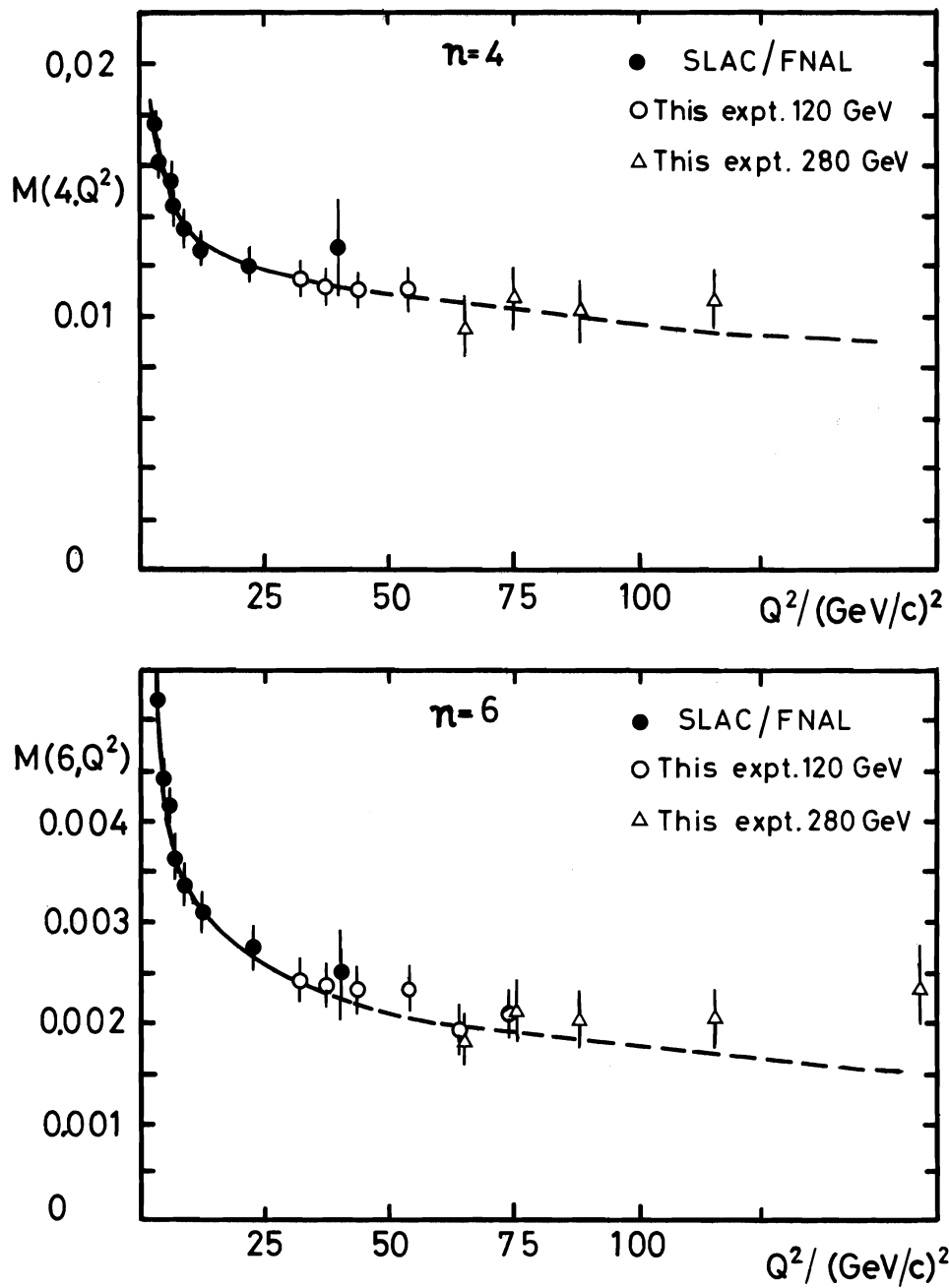


Fig. 16. Measurement of the Nachtmann moments for $n = 4, 6$. The dashed line is a fit to the SLAC and FNAL data only.